Tribology International 217 (2026) 111619

Contents lists available at ScienceDirect

Tribology International

journal homepage: www.elsevier.com/locate/triboint

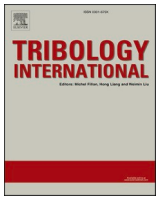

Influence of cross-shear and contact stress on the wear of UHMWPE on boost-diffusion-treated additively manufactured Ti-6Al-4V

L. Cremer [a], R.M. Cowie [b], J. van der Merwe [a,*], L.M. Jennings [b], T.H. Becker [c,*]

[a] Department of Mechanical and Mechatronic Engineering, Stellenbosch University, South Africa
[b] Institute of Medical and Biological Engineering, University of Leeds, United Kingdom
[c] Centre for Materials Engineering, University of Cape Town, South Africa

ARTICLE INFO

Keywords:
Wear testing
Multidirectional
Pin-on-Plate
Cross-Shear
Additive manufacturing
Ti-6Al-4V
UHMWPE

ABSTRACT

The more widespread adoption of additive manufacturing (AM) in the biomedical industry has enabled the production of patient-specific implants. When used in joint replacements (or as a bearing material), it is essential to understand the wear behaviour of additively manufactured implants when subjected to loading and motion that simulate their intended use. The aim of this study was to investigate the influence of cross-shear and contact stress on the wear behaviour of ultra-high molecular weight polyethene (UHMWPE) against boost-diffusion-treated (BD-treated) AM Ti-6Al-4V under varying conditions. Multidirectional pin-on-plate wear testing was conducted across cross-shear ratios from 0 to 0.3 and contact stresses ranging from 0.56 to 14 MPa. Surface characterisation techniques were used before and after wear testing to gain insights into the wear mechanisms. The wear of UHMWPE against BD-treated Ti-6Al-4V was compared to that of CoCr and untreated wrought Ti-6Al-4V. Results revealed that against BD-treated Ti-6Al-4V, UHMWPE wear was initially high due to the high surface roughness; however, continued wear testing led to polishing of the BD-treated Ti-6Al-4V, a reduction in the dynamic friction coefficient, and a decrease in wear rate. The high initial surface finish of the BD-treated Ti-6Al-4V resulted from the oxidation heat treatments. However, following wear testing surface degradation was absent, highlighting the potential benefit of the surface treatment in AM patient-specific implants.

1. Introduction

Developments in the metal additive manufacturing (AM) field and subsequent post-manufacturing methods have facilitated the integration of AM into the production of medical implants [1]. Articulating joint implants can now be manufactured to include design features once unattainable through conventional manufacturing techniques [1–3]. Implants can be customised by tailoring the articulating and bone-implant surfaces to match the patient's anatomy. Furthermore, the mechanical properties of the implant can be modified by incorporating complex lattice structures, while improved osteointegration can be achieved through surface modifications that enhance bone on- and ingrowth [1,3,4].

Ti-6Al-4V alloy is one of the most commonly used AM alloys for biomedical applications due to its excellent biocompatibility, osteointegration, corrosion resistance, high strength-to-weight ratio, and superior mechanical properties [1–3,5,6]. However, one of the challenges when using Ti-6Al-4V within a bio-tribological environment, such as articulating joint implants, is its low wear resistance [3,6,7]. Thermal oxidation heat treatments have demonstrated promising results in enhancing the wear properties of Ti-6Al-4V by creating a hard rutile (TiO_2) oxide layer on its articulating surface [8]. The rutile layer also adds additional benefits, such as reduced bacterial infection [3], improved osteointegration [3,9,10], biocompatibility [10,11], and corrosion resistance [10,12,13]. However, the integrity of the adhesion of the oxide layer formed during the thermal oxidation treatment remains an issue due to the high Pilling-Bedworth ratio (the ratio of the volume of a metal oxide to the volume of the corresponding metal from which the oxide is created) of the rutile layer on Ti-6Al-4V [14]. Literature suggests that a gradual case hardening below the oxide layer through a heat treatment process known as boost diffusion (BD) can improve oxide layer adhesion [7,15–17]. The BD treatment facilitates the diffusion of oxygen into the Ti-6Al-4V through both substitution and interstitial sites, inhibiting dislocation movements and thereby increasing strength. Oxygen, a well-known α-phase stabiliser, contributes to increased hardness [7,15,16].

* Corresponding authors.
E-mail addresses: jovdmerwe@sun.ac.za (J. van der Merwe), thorsten.becker@uct.ac.za (T.H. Becker).

https://doi.org/10.1016/j.triboint.2025.111619
Received 18 September 2025; Received in revised form 18 December 2025; Accepted 22 December 2025
Available online 23 December 2025

The BD treatment typically consists of three steps: the first step involves an initial oxidation step whereby the material is placed in a furnace with an oxygen environment to grow a thin rutile layer at the gaseous/metal interface. This oxide layer acts as a reservoir during the second step, where the samples are placed in a vacuum furnace to facilitate oxygen diffusion into the Ti-6Al-4V substrate. In the third step, a final adherent oxide layer is grown by placing the samples back into a furnace with an oxygen environment [18,19].

BD treatments have been developed for wrought/cast Ti-6Al-4V [7,15], with a recent study conducted by Cremer *et al.* [20] developing a BD treatment for AM Ti-6Al-4V. Laser-based powder bed fusion (LPBF) Ti-6Al-4V with refined BD treatment parameters was used to create an adherent oxide layer. A case hardening depth of 215 μm was achieved with hardnesses of more than double the bulk hardness at the oxide/-substrate interface. The study recommended pre-clinical wear assessment as the next step in characterising the influence of a BD treatment on the wear properties of LPBF-produced Ti-6Al-4V.

Simple geometry, multidirectional pin-on-plate wear testing is a form of pre-clinical wear assessment, typically used to assess the wear properties of a new candidate material pair before whole joint wear characterisation is conducted. The ASTM F732 [21] standard outlines key aspects of pre-clinical wear testing, with multi-axial testing introduced into a recent revision of the standard. The importance of multi-axial wear testing to replicate in vivo joint motion was demonstrated by Wang [22], Wang et al. [23] and Turell et al. [24].

Multiple pin-on-plate wear test studies have since been performed on different material pairs, with different types of Ultra-High Molecular Weight Polyethylene (UHMWPE) articulating against wrought CoCr alloys, which are the most commonly used bearing couple in total joint replacements [21–24]. Kang et al. [25] found that the wear factor (K_f) of UHMWPE against CoCr is dependent on both cross-shear (*CS*) and contact stress. Limited studies have, however, been conducted on the pre-clinical wear assessment of UHMWPE on AM metals over a wide range of testing conditions. Different wear properties are expected for AM metals as the AM process influences the microstructure of the metal and, as such, the mechanical properties, such as hardness [26,27], which are known to influence wear.

Considering a broader spectrum of test conditions is crucial to determining which particular joint applications would yield acceptable wear properties, especially given the variety of possible patient-specific joint applications that can be pursued using AM methods. Some of the more prevalent patient-specific articulating joint implants being manufactured include the temporomandibular joint (TMJ) [28], knee joint [29], and ankle (talus) [30]. The wear characterisation of material pairs comprising AM metals is thus of great significance, given the growing use of AM in the biomedical industry along with innovations enabling more advanced implant designs. The novelty of the current study lies in establishing the wear response of UHMWPE against BD-treated AM Ti-6Al-4V within a clinically relevant CS and contact stress experimental design space.

This study aims to investigate the influence of *CS* and contact stress on the wear of a cross-linked UHMWPE pin on BD-treated LPBF Ti-6Al-4V plates. Using multi-axial pin-on-plate wear testing, a wide range of contact pressure and cross-shear conditions were assessed, with kinematic conditions informed by the TMJ and ankle. Furthermore, comparative wear experiments were conducted with cross-linked UHMWPE on CoCr and wrought untreated Ti-6Al-4V. Surface characterisation techniques were used before and after wear testing to gain insights into wear mechanisms.

2. Methods and materials

2.1. Pin-on-plate test parameters

Testing was performed with polymeric pins articulating against metallic plates as prescribed in ASTM F732. Fig. 1a shows the pin-on-plate experimental rig used, with Fig. 1b illustrating the workings of a single test station. Multidirectional motion was created through a rack-and-pinion mechanism, which rotates the pin about a fixed point while the plate reciprocates linearly over each wear cycle. A constant axial load was applied to the pin by using a weighted cantilever mechanism. Experiments were performed on a six-station pin-on-plate wear testing rig from the Institute of Medical and Biological Engineering (Leeds University, UK) [31–35].

A design-of-experiments approach was used to select the test conditions over the experimental design space, defined by *CS* and the contact stress. The *CS* bounds were determined by the capabilities of the pin-on-plate test rigs, which could achieve *CS* ratios between 0 (uniaxial motion) to 0.3. Contact stress (*P*) ranges were informed from the literature on the TMJ and ankle joints. Average TMJ contact stresses ranges between 0.56 and 3.80 MPa, with peak stresses of up to 13 MPa [36–38]. For the ankle joint, average contact stresses ranges between

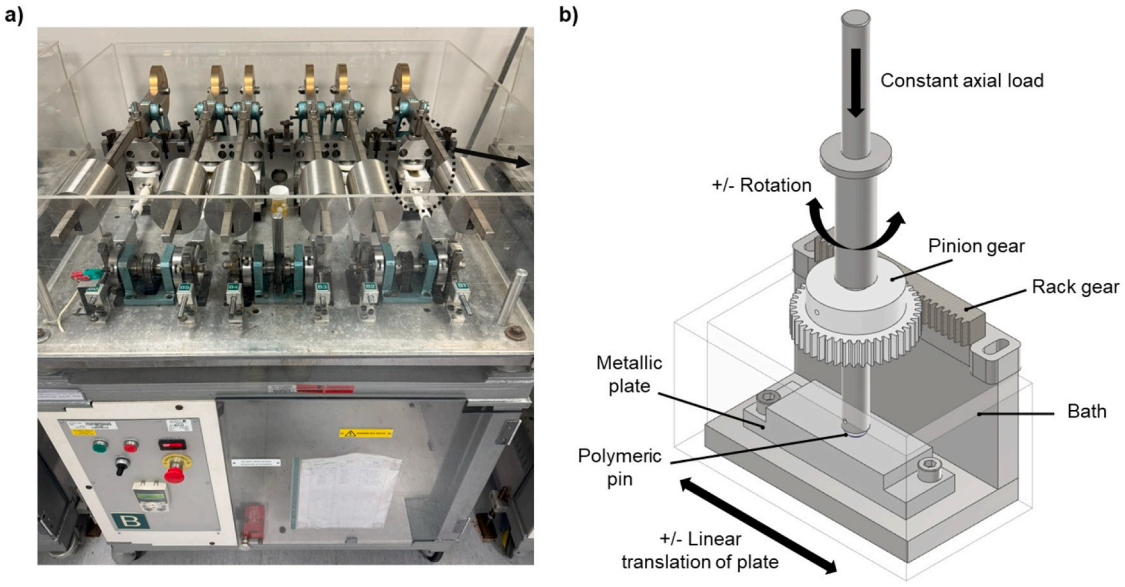

Fig. 1. a) Multidirectional pin-on-plate wear testing rig with b) a demonstration on the working principle of a single wear station utilising a rack and pinion mechanism.

1.20 and 5.10 MPa, with peak stresses up to 15 MPa [39–41]. The chosen contact stress range was thus 0.56–14 MPa, accommodating both joint contact stress ranges during pin-on-plate wear experiments.

A central composite design method was employed using the pyDOE2 module in Python (version 3.9.7) [42] to select the experimental runs that will be tested. Nine different load conditions were calculated and shown in Fig. 2 along with previous experimental runs found in the literature. These nine experimental runs were performed with moderately cross-linked GUR1020 UHMWPE (7.5 MRad) pins articulating against BD-treated LPBF-produced Ti-6Al-4V plates (this material pair is hereafter referred to as BD with the corresponding run number, as indicated in Fig. 2). Additionally, the central design point (BD-5) was repeated with moderately cross-linked UHMWPE pins articulating against wrought CoCr plates (material pair is hereafter referred to as CoCr) as well as wrought untreated Ti-6Al-4V plates (material pair is hereafter referred to as Ti-6Al-4V).

Pin-on-plate machine parameters such as pin diameter, load, gear diameter, and stroke length for each loading condition were determined using the methods described by Cremer et al. [44]. The calculated pin-on-plate machine parameters are summarised in Table 1 along with the calculated central composite design points. A cycle frequency of 1 Hz was used during all tests, with the amplitude of motion being fully reversed for each test cycle.

2.2. Test samples manufacturing

Each loading condition consisted of three metallic plates and four polymer pins, allowing for one unloaded soak control pin per experimental run. Test sample geometries are shown in Fig. 3. All pins were manufactured from moderately cross-linked GUR1020 UHMWPE (7.5 MRad) supplied by Orthoplastics (Lancashire, UK). Pins were machined to have contact surface diameters of 4 and 6 mm with an average surface roughness (R_a) of < 2 µm. Chamfers of 45° were included on the pins to alleviate edge effects during wear testing.

The BD runs used the BD-treated LPBF Ti-6Al-4V plates. The plates were manufactured at the Centre for Rapid Prototyping and Manufacturing - CRPM (Bloemfontein, South Africa), an ISO 13485 certified manufacturer, using standard printing parameters with the Z-build direction indicated in Fig. 3a. After printing, all plates underwent stress relieving (650℃ for 3 h followed by furnace cooling) and annealing (940℃ for 2 h followed by furnace cooling) heat treatments at CRPM using an SS12/24–13MDX T-M vacuum furnace (T-M Vacuum Products Inc., New Jersey, USA) operating at a vacuum level of $\sim 1.3 \times 10^{-4}$ Pa. The top articulating surfaces were then machined down and polished at the Centre for Materials Engineering (University of Cape Town, South Africa) to $R_a \sim 0.030$ µm using Struers polishing equipment (Struers, Copenhagen, Denmark).

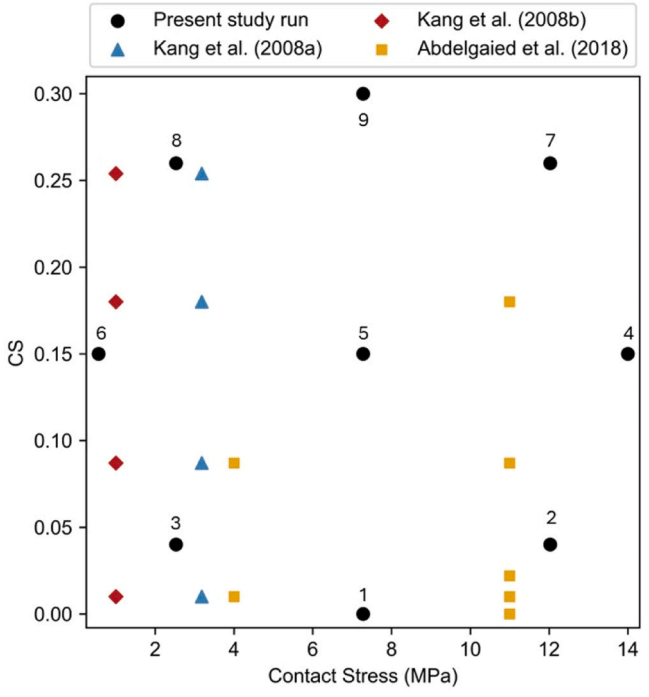

Fig. 2. BD experimental runs from the present study along with previous experimental runs investigated by Kang et al. (2008a) [34], Kang et al. (2008b) [25] and Abdelgaied et al. (2018) [43].

After polishing, all LPBF Ti-6Al-4V plates underwent the BD heat treatment, as summarised in Table 2, previously developed by Cremer *et al.* [20]. Heat treatments were again performed at CRPM with the first and third steps carried out in air using a Nabertherm LH 120/12 furnace (Nabertherm GmbH, Lilienthal, Germany). The second diffusion step was performed in a vacuum, using the same T-M vacuum furnace as previously mentioned.

In addition, control tests comprising three wrought untreated Ti-6Al-4V and three wrought CoCr plates were machined and polished to $R_a \sim 0.020$ µm using Struers polishing equipment (Struers, Copenhagen, Denmark). These samples would aid in directly comparing the wear properties of UHMWPE on BD, CoCr, and Ti-6Al-4V.

2.3. Wear studies

Before commencing with wear testing, all pins were soaked in water for eight weeks to stabilise the moisture content. The lubricant used during testing was 25 % bovine serum (protein concentration ~16 g/l) with 0.03 % sodium azide solution (v/v) added to inhibit bacterial growth. No external heating was applied to the lubricant baths during testing, with the studies carried out at the running temperature of the rig (~25 ℃), to reduce test artefacts such as protein deposition and degradation [32,45]. All BD test runs ran for two weeks (~600 000 cycles), with BD-5, BD-3, CoCr, and Ti-6Al-4V studies extended to four weeks (~1 200 000 cycles).

Each station was thoroughly cleaned after one week of testing with standard detergent, then Chemgene HLD_4L, followed by ultrasonic cleaning in 70 % water diluted isopropanol. After cleaning, the pins were left for 48 h to stabilise in a temperature (20 ± 1℃) and humidity (50 ± 5 %) controlled room, after which wear was gravimetrically assessed.

A Mettler XP26 digital microbalance (Mettler Toledo, Leicester, UK) was used to measure the pins' mass. Mass measurements were repeated until five consecutive measurements fell within ± 5 µg. Soak control samples were used to correct mass measurement changes due to moisture uptake during testing. The volumetric wear in mm^3 (ΔV) was then calculated by dividing the change in pin mass with the density of GUR 1020 of 0.937 g/cm^3. Additionally, wear was defined by calculating the wear factor (K_f) and wear coefficient (K_c) using [46]:

$$K_f = \frac{\Delta V}{Fs}, \text{ and} \quad (1)$$

$$K_c = \frac{\Delta V}{As}, \quad (2)$$

where F is the load (N), s the sliding distance (m) and A the nominal contact area (mm^2).

Wear results were analysed using Design-Expert version 23.1 (Stat-Ease, Minnesota, United States) to formulate response surfaces for ΔV, K_f and K_c over the BD testing matrix. Averages were calculated for each load case analysed. In addition, trend lines (linear and power fits) were generated for wear results from extended testing of BD-3, BD-5, Ti-6Al-4V and CoCr using Excel, version 2408 (Microsoft, Washington, United States).

Statistical significance was determined by using single factor ANOVA

Table 1
Pin-on-plate experimental study parameters.

Run	Contact Stress [MPa]	CS	Pin Diameter [mm]	Load [N]	Gear diameter [mm]	Stroke [mm]
BD-1	7.28	0	6	206	-	18.6
BD-2	12.00	0.04	4	151	55	19.0
BD-3	2.53	0.04	6	71.5	55	18.6
BD-4	14.00	0.15	4	176	36	25.2
BD-5	7.28	0.15	6	206	55	38.5
BD-6	0.56	0.15	6	15.9	55	38.5
BD-7	12.00	0.26	4	152	36	34.8
BD-8	2.53	0.26	6	71.5	36	34.7
BD-9	7.28	0.30	6	206	36	38.0
CoCr	7.28	0.15	6	206	55	38.5
Ti-6Al-4V	7.28	0.15	6	206	55	38.5

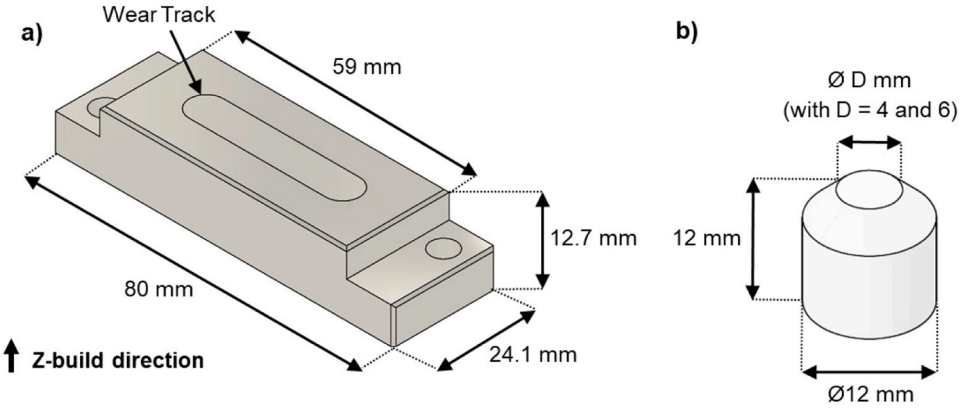

Fig. 3. Test sample geometries for a) metallic plates and b) polymer pins. The intended wear track is illustrated on the plate articular surface.

Table 2
Boost diffusion heat treatment.

	Temperature (C)	Holding time (hours)	Furnace environment	Cooling method
Step 1: Short Oxidation	680	0.5	Air	Furnace cool
Step 2: Diffusion	850	20	Vacuum	Furnace cool
Step 3: Long Oxidation	600	20	Air	Furnace cool

with $\alpha = 0.05$. Post hoc analysis was performed using Tukey's honestly significant difference with $\alpha = 0.05$ in cases where the ANOVA analysis found statistical significance.

2.4. Surface characterisation

The R_a, mean surface roughness, was measured post-testing by using a contacting Form TalySurf (Taylor Hobson, Leicester, UK) equipped with a 2 μm conical stylus tip. All measurements were taken with the appropriate filters and cutoffs applied, in accordance with ISO 21920–3 and the specific material. Plate surface roughness's were measured beside the wear track, as well as parallel and perpendicular to the major principal axis of the wear track. The surface roughness of the pins was measured by taking two orthogonal measurements over the articular surface and calculating the average.

Articulating surfaces of the polymer pins were imaged using an Alicona G5 optical microscope (Alicona, Graz, Austria) to identify key wear mechanisms. BD plates were analysed using scanning electron microscopy (SEM), with elemental composition analysis being performed by making use of energy-dispersive X-ray spectroscopy (EDS) on a Tescan MIRA 3 (Tescan Group, Brno, Czechia). SEM analysis was performed by making use of the secondary electron detector. Throughout the SEM analysis, a constant voltage of 20 kV was used.

2.5. Friction

A pin-on-plate friction test rig from the Institute of Medical and Biological Engineering (Leeds University, UK) was used to determine dynamic friction coefficients for the different material pairs considered in this study. Material pairs studied included moderately crosslinked UHMWPE pins articulating against unworn BD, CoCr, Ti-6Al-4V, and post-test BD-1 and BD-9 plates.

The test setup has been previously described by Foster and Fisher [47] and more recently by Cowie *et al.* [32]. Fig. 4 shows the basic workings of the friction test rig. Uniaxial linear reciprocating motion was used, where the plate moves linearly while the pin remains stationary within a pivot bridge. Both the pin and the plate are housed inside an unheated bath with 25 % bovine serum and 0.03 % sodium azide solution. The start of test lubricant temperature was ~ 26.5C. The plate was linearly actuated with a crank arm mechanism, which had a stroke of 20 mm and 0.5 Hz frequency. Tests ran for 10 min and were repeated three times per material pair. A constant axial load of 205.8 N was applied to the pin using a cantilever mechanism, resulting in a contact pressure of 7.28 MPa.

A piezoelectric force sensor was mounted on the pivot bridge to measure the friction force (F_R) of the pin as the plate reciprocates. The output voltage from the sensor was collected using LabView (National Instruments, Texas, United States) and converted to F_R using a calibration factor to account for friction and geometry within the setup. The following equation was used to calculate the dynamic friction coefficient (μ):

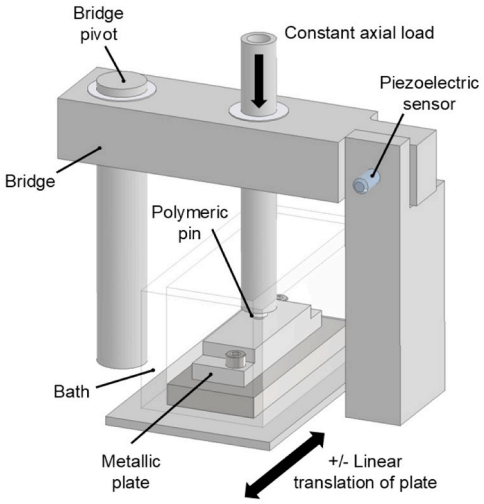

Fig. 4. Illustration showing the workings of the friction test rig used.

$$\mu = \frac{F_R}{F_N}, \tag{3}$$

with F_N the normal reaction force to the applied load (N).

3. Results

3.1. BD wear studies

The fitted response surface equations for ΔV, K_f and K_c are summarised in Table 3, along with the respective R^2 values after ~600,000 cycles. ΔV, K_f and K_c were best described using quadratic models with respect to *CS* and *P* variables. The obtained R^2 values were consistent with those reported in previous studies, which typically ranged between 0.6 and 0.9 [25,34,48]. Model significance was evaluated using analysis of variance (ANOVA) in Design-Expert. The fitted quadratic models achieved the following results ΔV ($F = 4.27$, $p = 0.13$), K_f ($F = 1.38$, $p = 0.42$), and K_c ($F = 10.15$, $p = 0.04$). These results confirmed that the model for K_c was statistically significant ($p < 0.05$), while the remaining models show acceptable fits, but did not reach statistical significance within the tested design space. The corresponding response surfaces for ΔV, K_f and K_c are shown in Figs. 5–7.

It is well known that *CS* has a significant influence on the wear of UHMWPE [22,34]. From Fig. 5a, the non-linear relationship between *CS*, *P*, and ΔV is evident from the curvature observed in the contour lines. Fig. 5a shows that ΔV increases with *CS* and *P*. This wear behaviour is supported by literature, which reported that ΔV increases as *CS* increases for UHMWPE on CoCr [34]. In addition, contour intervals narrow with higher *CS* and *P* values, indicating a more rapid increase in the rate of change of ΔV. As a result of this wear behaviour over the test region, namely different rates of change of ΔV, a convex response surface is seen in Fig. 5b.

Table 3
BD response surface equations for ΔV, K_f and K_c as a function of *CS* and *P*.

Wear indicator	Equation				R^2
ΔV	$\Delta V(CS,P) = a + b.P + c.CS + d.P.CS + e.P^2 + f.CS^2$			(4)	0.88
	$a = 0.118$	$b = 1.83$	$c = 12.5$		
	$d = 6.73$	$e = -0.129$	$f = 18.9$		
K_f	$K_f(CS,P) = a + b.P + c.CS + d.P.CS + e.P^2 + f.CS^2$			(5)	0.70
	$a = 7.08E-06$	$b = -1.35E-06$	$c = -3.04E-06$		
	$d = 9.651E-07$	$e = 7.22E-08$	$f = -6.85E-07$		
K_c	$K_c(CS,P) = a + b.P + c.CS + d.P.CS + e.P^2 + f.CS^2$			(6)	0.94
	$a = 1.12E-08$	$b = -2.19E-09$	$c = -7.41E-08$		
	$d = 6.55E-09$	$e = 2.84E-10$	$f = 2.17E-07$		

Table 4
Equations fitted to ΔV over the cycles completed (x) with the corresponding R^2.

Material pair	Equations for $\Delta V(x)$ [mm^3]			R^2
BD-3	Linear:	$\Delta V(x) = 7.32x$	(7)	0.96
	Power:	$\Delta V(x) = 7.431x^{0.667}$	(8)	0.97
BD-5	Linear:	$\Delta V(x) = 19.87x$	(9)	0.97
	Power:	$\Delta V(x) = 20.99x^{0.55}$	(10)	0.99
Ti-6Al-4V	Linear:	$\Delta V(x) = 3.45x$	(11)	~1
CoCr	Linear:	$\Delta V(x) = 0.88x$	(12)	~1

Normalising ΔV to the applied load and sliding distance (Eq. 1) calculates K_f. Fig. 6a shows that there is similarly a non-linear relationship between *CS*, *P* and K_f, with a valley located at a *P* of 8 MPa. The valley, along with BD test points, can be seen in Fig. 6b. Moving away from the central valley, K_f increases, indicative of increased wear. In the region where $P < 4$ MPa, K_f shows greater sensitivity to changes in *P*, as demonstrated by the close spacing of contour lines in Fig. 6a. For $P > 10$ MPa, K_f shows less sensitivity to changes in *P*. Similarly, a study by Kang *et al.* [25] on the wear of GUR 1050 UHMWPE on CoCr for contact stress ranges of 1–10 MPa and *CS* ranges between 0 and 0.25, showed that K_f increased more significantly for lower contact stresses. Furthermore, the contours from Fig. 6a indicate that K_f is less sensitive to *CS* than *P*, reflected in the relatively low variability of K_f across different *CS* values. This observation is largely due to the cross-linking of the UHMWPE, which has been shown to reduce the effects of *CS* on the wear of the polymer [34].

K_c, a non-dimensional value, is calculated by normalising ΔV for the applied load and nominal contact area (Eq. 2). The wear behaviour over the test range, shown in Fig. 7a and b, resulted in a concave K_c response surface. The contours in Fig. 7a show that K_c is more sensitive to a change in *P* compared to *CS*, as indicated by the contour spacing decreasing more significantly as *P* increases when compared to *CS*. Fig. 7a shows the non-linearity of the response surface, with curved contour lines. The relationship for K_c as a function of *CS* and *P* can thus be described by stating that an increase in both *CS* and *P* will lead to an increase in K_c. Abdelgaied *et al.* [43] found that K_c is dependent on both *CS* and *P* for moderately crosslinked UHMWPE on CoCr, which is in agreement with the findings from the present study. A relatively flat K_c region was found for $P < 7$ MPa, indicating a region where the wear behaviour is more constant for different *CS* and *P* values.

Overall, the wear behaviour observed over the BD test matrix exhibited similar trends to those reported in literature for UHMWPE on CoCr [25,43,46], particularly regarding the relationships between *CS* and *P*, and their influence on ΔV, K_f and K_c. Higher wear than expected was found, particularly when compared with pin-on-disc wear testing performed by Dong *et al.* [49], on UHMWPE against BD-treated wrought Ti-6Al-4V. Dong *et al.* [49] found a $K_f = 1.15E-8$ mm^3/Nm, compared to the minimum $K_f = 6.12E-7$ and maximum $K_f = 7.44E-6$ mm^3/Nm, as seen in Fig. 6b. Dong *et al.* [49], however, polished their BD-treated samples after surface hardening to reduce R_a from 0.200 to 0.030 μm before wear testing, as opposed to the current study, which did not repolish BD-treated samples after surface hardening, resulting in an $R_a \sim 0.060$ μm. Surface roughness is known to influence the wear of soft-on-hard material pairs, such as UHMWPE on BD-treated Ti-6Al-4V [46,50,51].

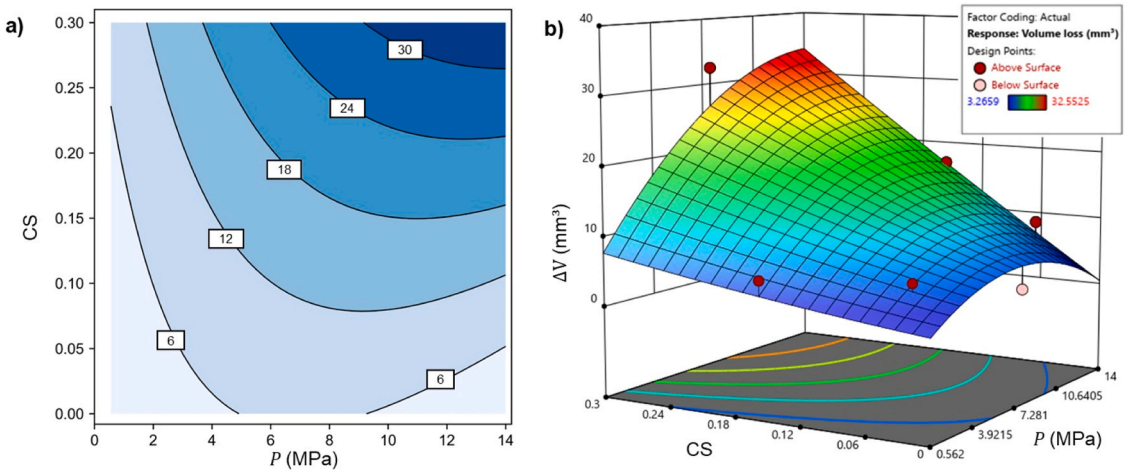

Fig. 5. a) Contour plot of ΔV (mm^3) as a function of *CS* and *P*, with b) showing a 3D representation of the response surface along with BD test points.

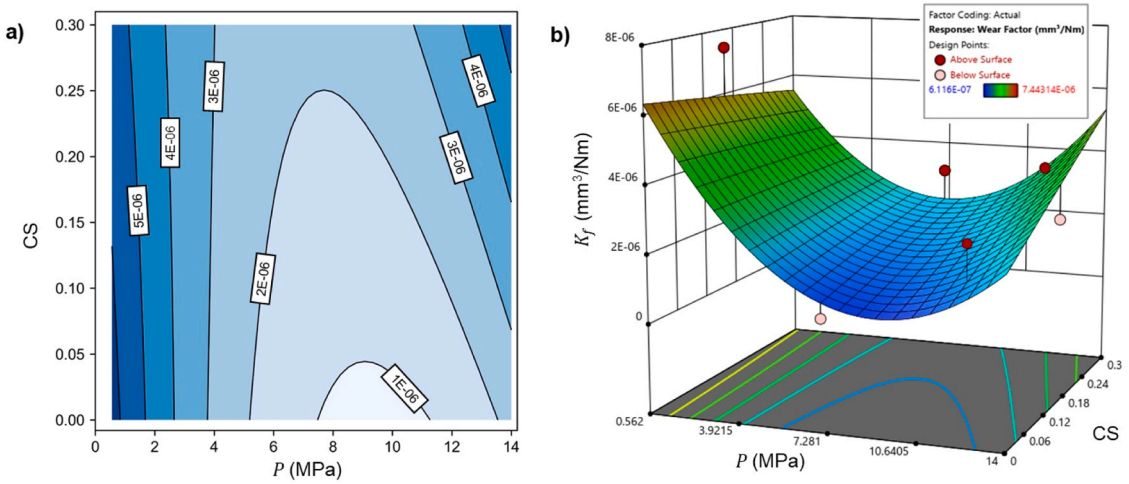

Fig. 6. a) Contour plot of K_f (mm^3/Nm) as a function of *CS* and *P*, with b) showing a 3D response surface representation along with BD test points.

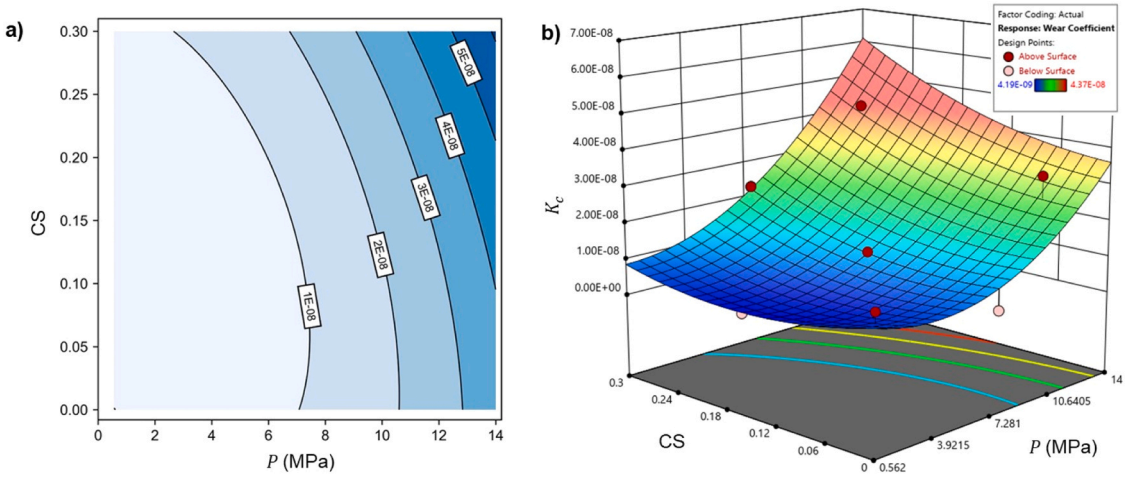

Fig. 7. a) Contour plot of K_c as a function of *CS* and *P*, with b) showing a 3D surface representation along with test points.

3.2. Extended wear testing

Fig. 8 shows ΔV, K_f and K_c over the wear cycles completed for BD-5 and BD-3, i.e., after ~1 200,000 cycles. The response of ΔV is shown in Fig. 8a-c. Linear fits demonstrated high accuracy for Ti-6Al-4V and CoCr material pairs with $R^2 \approx 1$. The linear fit for BD-3 and BD-5 was adequate over the extended test period, with $R^2 > 0.96$. However, initial ΔV measurements over the first ~600,000 cycles seemed higher than

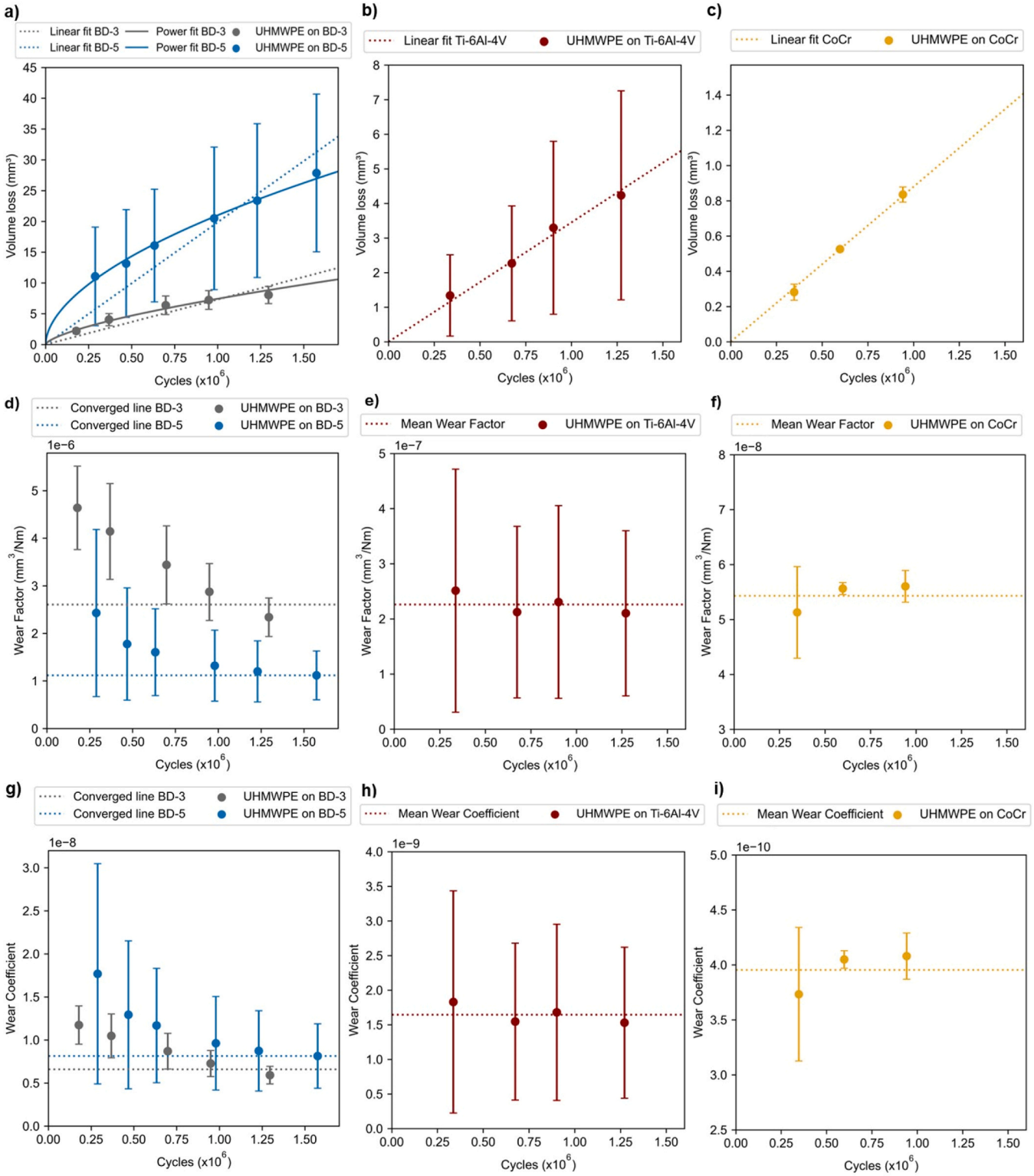

Fig. 8. Direct comparison showing the mean (± one standard deviation) of a-c) ΔV, d-f) K_f and g-i) K_c, for a,d,g) UHMWPE on BD-3, BD-5; b,e,h) UHMWPE on Ti-6Al-4V and c,f,i) UHMWPE on CoCr. Note: BD-5 was investigated under the same conditions as those used for Ti-6AL-4V and CoCr.

expected. A power law fit was applied to better capture the initial increase in ΔV, resulting in an improved $R^2 \approx 0.99$.

The initial elevated wear rates for BD-3 and BD-5 were also apparent in the K_f graph in Fig. 8d, which clearly shows a reduction in K_f as the number of wear cycles increased, eventually converging to a minimum value. BD-3 and BD-5 converged after ~600,000 cycles at K_f = 2.61E-06 mm³ /Nm and K_f = 1.12E-06 mm³ /Nm, respectively. Ti-6Al-4V and CoCr material pairs had constant K_f over the extended test period, resulting in K_f = 2.26E-07 mm³ /Nm and K_f = 5.43E-08 mm³ /Nm for Ti-6Al-4V and CoCr material pairs, respectively, as shown in Fig. 8e and f.

The decrease in wear rate for BD-3 and BD-5 over the initial cycles of

the study was further highlighted when considering K_c in Fig. 8g. BD-3 and BD-5 each converged at K_c= 6.59E-09 and K_c = 8.14E-09, respectively, after ~600,000 cycles. Ti-6Al-4V and CoCr showed constant K_c values over the extended test period as K_c = 1.65E-09 for Ti-6Al-4V and K_c = 3.95E-10 for CoCr.

By using a fitted response surface for GUR1020 UHMWPE (5 MRad) on CoCr generated by Abdelgaied *et al.* [43], the expected K_c for the CoCr material pair can be estimated at the same *CS* and *P* from the current study as K_c = 1.34E-09. Cremer *et al.* [52] tested conventional UHMWPE plates articulating against LPFB CoCr pins at a CS of 0.1 and *P* equal to 2.53 MPa and found a K_f of 3.61E-07 mm^3 /Nm. In addition, K_f = 2.26E-07 mm^3 /Nm of the Ti-6Al-4V material pair is also lower than previous reported K_f for UHMWPE (GUR4150HP) on untreated Ti-6Al-4V of 3.77E-06 mm^3 /Nm [49]. These lower K_c and K_f found in the present study for the CoCr and Ti-6Al-4V material pair, is likely a consequence of the higher irradiation dose of 7.5 MRad and consequent cross-linking in the GUR1020 UHMWPE. An increased irradiation doses have been shown to decrease wear in UHMWPE [22,34,53].

Statistical analyses were performed on end-of-test K_f and K_c data points for each material pair (n = 9). Analysis of K_f found a statistical significance between BD-5 and Ti-6Al-4V ($p < 0.01$), as well as CoCr ($p < 0.05$). Similarly, analysis of K_c found statistical significance between BD-5 and Ti-6Al-4V ($p < 0.01$), as well as CoCr ($p < 0.01$). The BD-5 material pair had lower wear resistance compared to Ti-6Al-4V and CoCr. Considering ΔV, K_f and K_c, the wear performance can be ranked; the CoCr material pair outperformed Ti-6Al-4V and BD-5 across all three wear indicators. Second was Ti-6Al-4V, followed by BD-5. The surface characterisation section to follow aims to provide insight into the observed wear behaviour.

3.3. Surface characterisation

The articulating surfaces of BD-treated (BD-5) and Ti-6Al-4V are shown in Fig. 9 after ~600,000 cycles. Fig. 9b clearly shows how the untreated Ti-6Al-4V plates exhibited significant scratching over the wear track (region 2), in contrast to the BD-treated plates in Fig. 9a, which showed no signs of scratching (region 1). Dong *et. al* [49] also found severe surface degradation of untreated Ti-6Al-4V articulating against UHMWPE after wear testing, with deep abrasive wear on the UHMWPE. Minor dark spots were identified on the BD plates (region 3 in Fig. 9a), resulting from the thermal oxidation heat treatment, which can lead to localised oxide grain clusters [15], thereby increasing surface roughness. On average, the initially polished AM Ti-6Al-4V plate surface roughness increased from R_a = 0.030 μm to R_a = 0.065 μm, following the BD-treatment.

As part of the initial surface characterisations, the surface roughness of both BD-treated plates and the polymer pins were measured after ~600,000 cycles of wear testing. Fig. 10 summarises the R_a for plates and pins over the BD experimental runs. It can be seen from Fig. 10a, that following wear testing, the R_a of the tested plates were lower than pre-test measurements. The surface roughness decreased in both perpendicular and parallel directions, with a more notable improvement observed over all test runs in the parallel directions, which is the principal sliding direction. The mean R_a for the BD plates were calculated to be 0.064, 0.056, and 0.053 μm for the untested plate, tested plate perpendicular and parallel to the wear track, respectively. Similarly, the Ti-6Al-4V plates have R_a values of 0.012, 0.186, and 0.095 μm, respectively. The scratching on the surface of the untreated Ti-6Al-4V plates (as seen in Fig. 9b) is likely a contributing factor to the increase in surface roughness of the plates.

Measured pin R_a values after the BD runs are shown in Fig. 10b. The values were measured to be ~1.000 μm before testing. The mean R_a of the BD pins was calculated to be 0.580 μm after ~600 000 cycles, showing reduction after wear testing, which is to be expected since machining marks are polished away. In addition, the pins from the Ti-6Al-4V pairing had a R_a of 1.320 μm after ~600 000 cycles, as shown in Fig. 10b, suggesting that the surface roughness increased after articulating against the untreated Ti-6Al-4V plate. This could be due to deeper abrasive scratches on the pin surface, as reported by Dong *et. al* [49], leading to higher surface roughness.

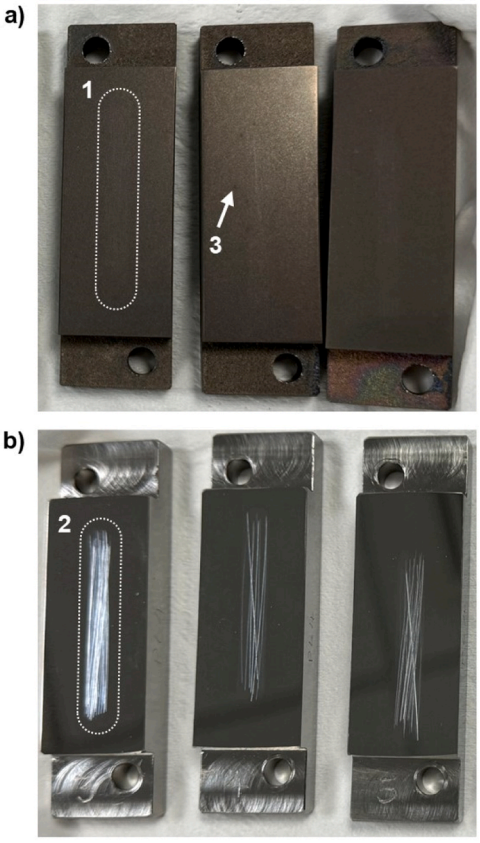

Fig. 9. Articulating surface images after ~600,000 cycles of wear testing for a) BD-treated and b) untreated Ti-6Al-4V plates.

Similarly, R_a measurements for BD-3, BD-5 and Ti-6Al-4V plates were taken after ~1 200 000 cycles and are presented in Fig. 11. Notably, the Ti-6Al-4V plate surface roughness increased, resulting in R_a values of 0.012, 0.187 and 0.085 μm measured before testing, perpendicular and parallel to the wear track after testing, respectively. Furthermore, the R_a values after ~1 200 000 cycles were similar to those after only ~600 000 cycles, suggesting no further surface topography changes occurred.

Fig. 12 shows the articulating surface of a polymeric pin after articulating against a BD plate after ~600 000 cycles. Region A shows how machining marks typically seen on untested polymeric pins are polished away after testing. This was also supported by the decrease in R_a after wear testing. As shown in Fig. 12, small (arrow 1) and larger (arrow 2) abrasive wear tracks are evident and as such abrasive wear was identified as the primary wear mechanism on the polymer pins.

Higher magnification SEM images of the BD plates, both within and outside the wear track, are shown in Fig. 13. The surface morphology, outside the wear track in Fig. 13a, comprises densely packed polyhedron-type oxide grains. It was observed that the underlying microstructure of the Ti-6Al-4V appeared to result in varying protrusion levels of the oxide grains. Interestingly, post-wear testing plates revealed that asperities visible outside the wear track were smoothed within the wear track, leading to an improved surface roughness, as seen in Fig. 13b. This observation is corroborated by Fig. 10a, where the R_a reduced after wear testing due to the continued tribological contact of the polymeric pin on the BD plate. The lower surface roughness over the

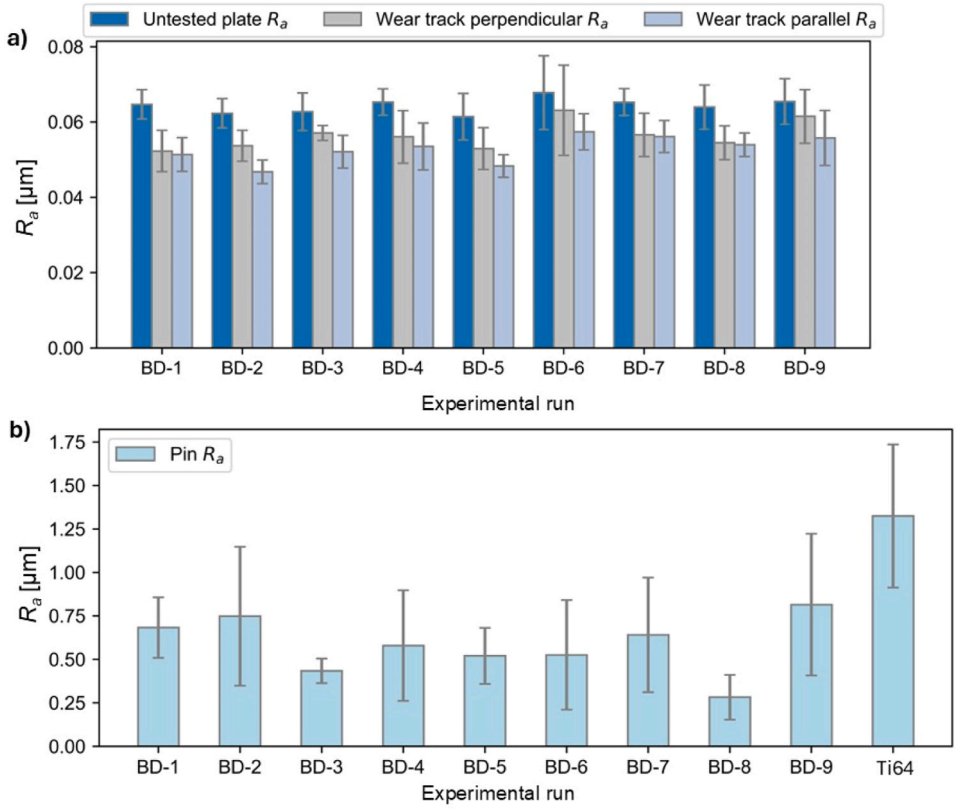

Fig. 10. Bar plot with + /- one standard deviation showing a) the mean R_a before testing and after ~600 000 cycles parallel and perpendicular to the main linear sliding direction, along with a bar plot of b) the mean pin R_a for the respective BD and untreated Ti-6Al-4V wear couples.

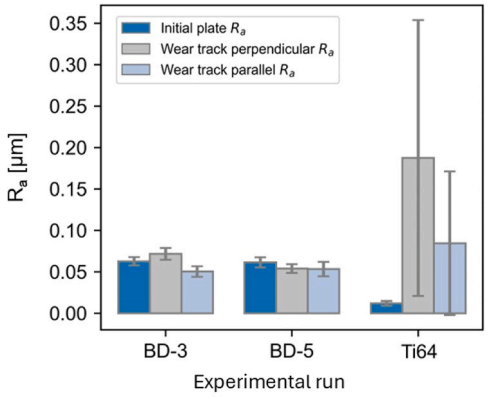

Fig. 11. Bar plot showing the mean R_a + /- one standard deviation, before and after extended wear testing within the wear track, parallel and perpendicular to the main linear sliding direction.

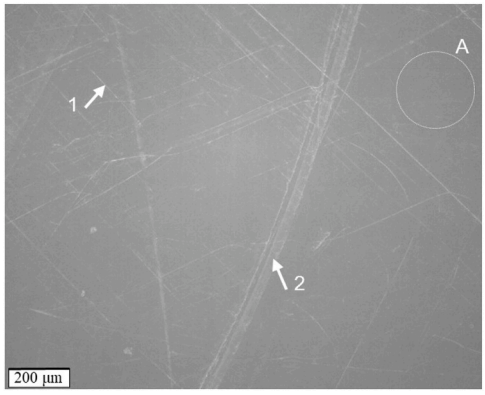

Fig. 12. Articulating surface of a UHMWPE pin against BD plate after 600,000 cycles. Taken with an Alicona G5 optical profiler at 10X magnification.

duration of the wear test is hypothesised to have lowered K_f and K_c after ~600,000 cycles, as seen in Fig. 8d and g.

Small protruding asperities (10–100 µm in diameter) were identified on the surface of the BD plates, as seen in Fig. 9a. This is a common drawback when using thermal oxidation, where the surface finish degrades after heat treatment, mainly due to oxide grain clusters forming protrusions of up to 2 µm on the surface [15]. SEM-EDS composition maps were used to investigate the elemental composition of one of these oxide clusters.

Fig. 14 shows an unworn BD plate surface, an oxide grain cluster, and the resulting elemental composition maps for O, Ti, V, and Al. The elemental distribution in Fig. 14a was 41.7 wt% O, 52.7 wt% Ti, 1.9 wt % V, and 3.7 wt% Al. Localised areas with higher O-concentrations and lower Ti-concentrations can be seen to form at grain boundaries in Fig. 14a, resulting in some of the more prominent oxide grains seen in Fig. 13a. Fig. 14b shows one of the oxide grain clusters with the elemental distribution of 42.3 wt% O, 52.2 wt% Ti, 1.9 wt% V, and 3.6 wt% Al. Slightly higher Ti and V concentrations can be seen within the oxide grain cluster region in Fig. 14b. A localised spectrum within the oxide grain cluster region revealed ~8 wt% higher Ti and ~4 wt% higher V, compared to the overall region, possibly leading to the protrusion and higher surface roughness.

Minor instances of localised delamination, shown in Fig. 15, were observed in samples subject to more extensive loading conditions (higher contact stress and CS). However, the oxide layer delamination was contained within these regions, with edges polished down along the main sliding direction during wear testing (indicated region in Fig. 15),

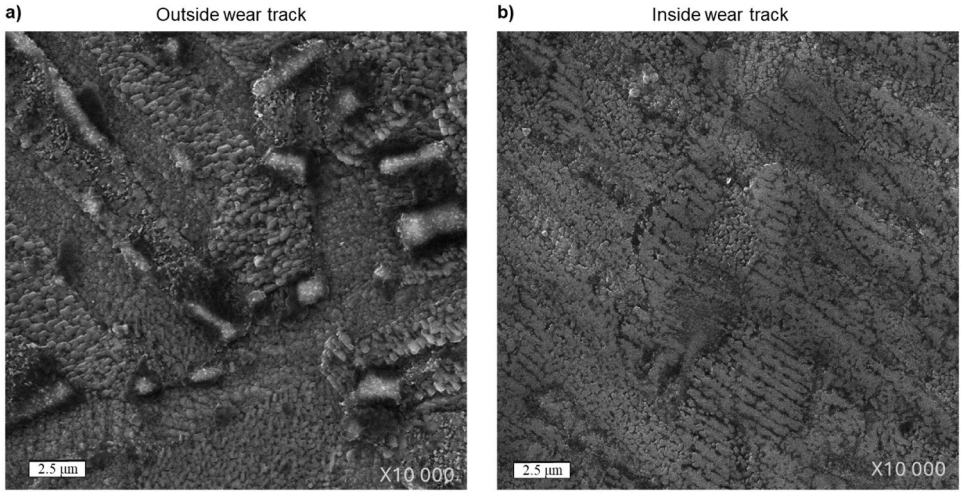

Fig. 13. Articulating surface of BD plate **a)** outside and **b)** inside the wear track at x10 000 magnification.

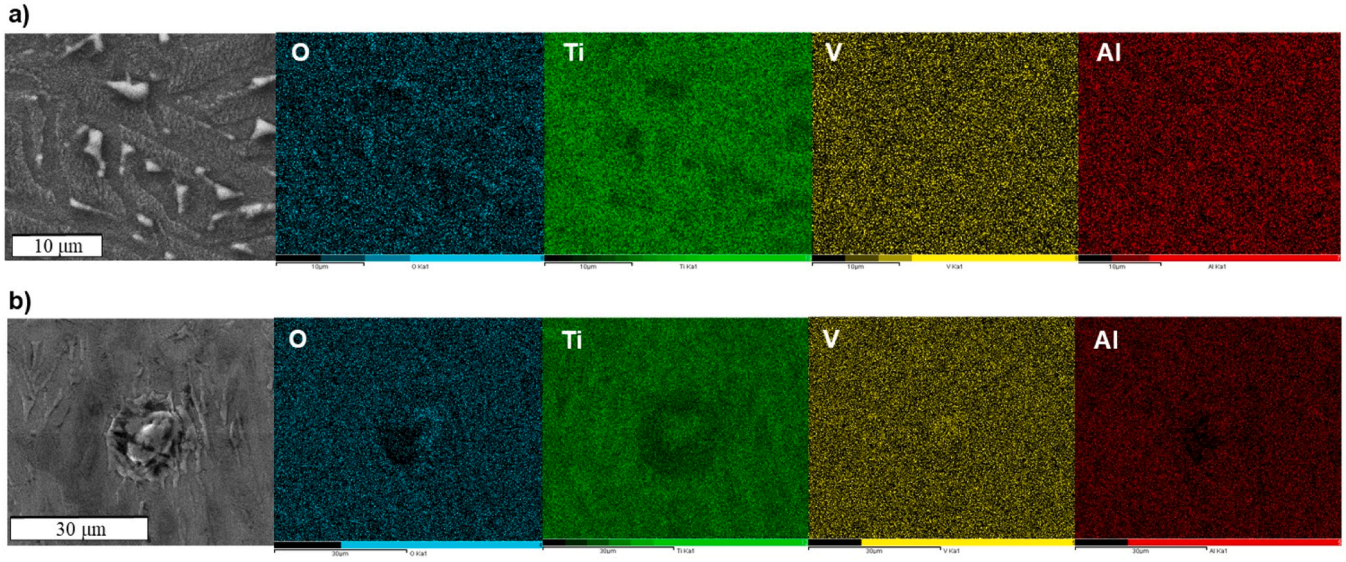

Fig. 14. SEM EDS composition maps of **a)** the BD plate articulating surface and **b)** an oxide grain cluster formation.

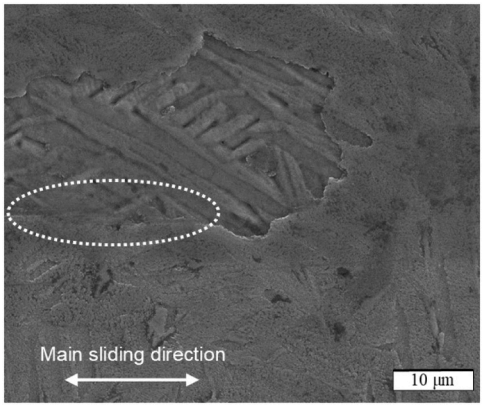

Fig. 15. High magnification SEM image of a BD plate wear feature (instance of localised delamination).

demonstrating the enhanced adhesion achieved by using a boost diffusion treatment. Furthermore, it is theorised that these localised delamination areas formed as a result of the polishing of some more prominent oxide grain clusters during wear testing. Similar delamination features were found by Dong *et al.* [6], following wear testing of thermally oxidised Ti-6Al-4V.

3.4. Friction

The dynamic friction coefficient was determined for unworn BD plates, post-test BD, Ti-6Al-4V, and CoCr plates after ~600,000 cycles. The resulting friction coefficients are summarised in Fig. 16. The CoCr material pair had the lowest coefficient of friction of 0.03. Second was the Ti-6Al-4V material pair with 0.07, followed by the BD-1 with 0.18, BD-9 with 0.21, and the untested BD material pair with 0.34. It was clear that the untested BD plate had a notably higher friction coefficient than post-test BD plates. This could have contributed to the reduction in wear of the BD plates over wear testing. Statistical analysis indicated a significant difference among all material pairs ($p < 0.01$), except between BD-1 and BD-9.

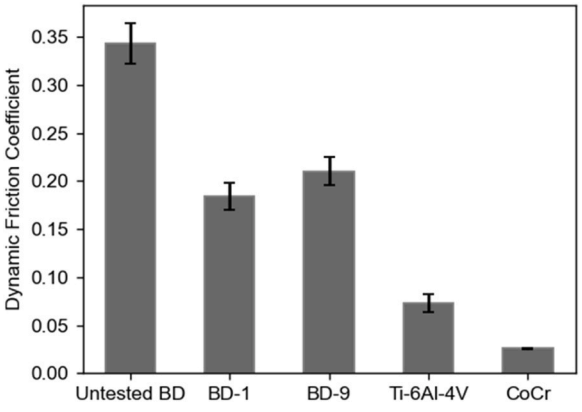

Fig. 16. Dynamic friction coefficient (± one standard deviation) after 600,000 cycles for BD-1, BD-9, Ti-6Al-4V and CoCr as well as on an untested BD plate.

4. Discussion

This study aimed to investigate the influence of cross shear and contact stress on the wear of cross-linked UHMWPE on BD-treated LPBF Ti-6Al-4V. Simple geometry, multidirectional pin-on-plate wear testing was conducted, along with surface characterisation techniques, to provide insights into the observed wear behaviour. This study also considered Ti-6Al-4V and CoCr material pairs to facilitate direct comparison between different material pairs.

Key wear indicators, including ΔV, K_f, and K_c, were characterised using response surfaces to show how the wear of BD material pairs is influenced by *CS* and *P* values. *CS* ranged from 0 to 0.3 and *P* from 0.56 to 14 MPa. It was found that quadratic response surfaces achieved good fits over the test range, achieving $R^2 > 0.7$. *CS* and *P* were found to have a non-linear impact on ΔV, K_f and K_c. Overall, the wear behaviour of the BD material pair aligned with trends reported in the literature for UHMWPE on CoCr [25,43,46], particularly in relation to the influence *CS* and *P* has on ΔV, K_f and K_c.

The ΔV response surface showed that as *CS* and *P* increases, ΔV increases, which is consistent with findings from literature [34]. The response surface for K_f showed a clear valley at $P \approx 8$ MPa, with K_f increasing when moving away from the valley. This possibly indicates a region where the wear behaviour could be favoured, due to lower K_f. It was also found that K_f increased more significantly for lower contact stresses ($P < 4$ MPa), as was also found by Kang *et al.* [25]. The K_c response surface was found to be proportional to *P* and *CS* with K_c increasing with an increase in *P* and *CS*. This was also observed by Abdelgaied *et al.* [43]. For $P < 7$ MPa, a relatively flatter K_c was found indicating a region where the wear behaviour is more constant for changing *CS* and *P* values. Both K_f and K_c were found to be more sensitive to change in *P* compared to *CS*, over the entire test region, which is largely attributed to the crosslinking of the UHMWPE, which is known to improve the wear properties of UHMWPE under multidirectional motion (i.e., CS) [34].

Extended wear testing revealed that the wear of both BD-3 and BD-5 decreased over the initial ~600,000 cycles (Fig. 8). This was an unexpected observation, given that the CoCr and Ti-6Al-4V material pairs showed consistent wear behaviour with a linear ΔV, and constant K_f trend K_c as cycles increased, consistent with literature [34,52]. Surface characterisation of the BD plates showed that the polymer pins polished the BD-treated plates over wear testing, thus decreasing the wear rate over the duration of the study. The polishing effect was highlighted by the surface roughness reducing after wear testing for the BD plates, as shown in Fig. 10a and Fig. 11. Likely as a result of the lower surface roughness, the resulting dynamic friction coefficient also decreased. Fig. 15 shows that the tested BD plates had a friction coefficient ~43 % lower than untested BD plates. Furthermore, Fig. 13 illustrates the polishing of the thermal oxide layer, where oxide grain formations within the wear track were flattened, in contrast to outside the wear track.

It is argued that the higher surface roughness of the BD plates was the main contributing factor to the elevated wear observed in the BD material pair. Especially given the low wear factor reported by Dong *et al.* [49], who polished their wrought Ti-6Al-4V plates after BD-treatment from $R_a = 0.200$–0.030 μm. The roughness of the BD plates from the present study increased from $R_a = 0.030$–0.064 μm following BD-treatment and were not repolished following heat treatment. Repolishing to an R_a of 0.030 likely will yield improved wear properties, exceeding that of the wrought material, but this will need to be confirmed in a follow up study. Wear is a multifaceted phenomenon influenced by factors such as friction, lubrication regimes, and contact mechanics [54]. The elevated surface roughness could have led to a reduction of the effective lubricant film thickness, thereby leading to increased wear and asperity contact.

Surface characterisation of the BD plates highlighted possible factors contributing to the increased surface roughness post-BD heat treatment, including small protruding asperities shown in Fig. 9a and Fig. 14b. The protrusions were identified to be oxide grain clusters [15] with elevated Ti and V wt% compared to the overall region. Localised areas with more prominent oxide grains were also found in regions with higher O and lower Ti-consecrations, as seen in Fig. 13a and Fig. 14a. Both these factors contributed to the higher surface roughness post-BD heat treatment and could have led to the elevated wear rates reported during initial test cycles (< 600,000 cycles). This is since the pins would experience elevated abrasive wear in this region, due to the oxide grain clusters protruding from the plate articular surface, thus leading to higher wear of the polymer pin. Furthermore, due to the polishing effect the pin had on the BD plates, these elevated oxide grains are argued to be the cause of the minor instances of localised delamination found within the BD plate wear track (Fig. 15). Most notably, the delamination remained confined to these areas, with the edges polished down, demonstrating the improved adhesion of the oxide layer provided by the BD-treatment.

Direct comparison over extended wear testing revealed that the CoCr-UHMWPE material pair had the lowest wear factor, followed by Ti-6Al-4V then BD-5. The Ti-6Al-4V material pair had a lower $K_f = 2.26\text{E-}07$ mm^3 /Nm compared to literature, with $K_f = 3.77\text{E-}06$ mm^3 /Nm for UHMWPE (GUR4150HP) on untreated Ti-6Al-4V. In addition, the authors reported severe surface degradation of the untreated Ti-6Al-4V with deep abrasive wear on the UHMWPE [49]. In the current study, surface characterisation found significant scratching on untreated Ti-6Al-4V plates, with the mean surface roughness increasing from 0.012 to 0.186 μm perpendicular to the principle sliding direction, consistent with previous investigations [49]. Initial pin surface roughness's of $R_a \sim 1.000$ μm also increased after ~600 000 cycles of testing to 1.320 μm, with scratching visible on the pin.

The low wear rates for the Ti-6Al-4V compared to previous investigations can largely be attributed to the cross-linking of the polymer, which provides the GUR1020 polymer with high abrasion resistance [55]. Similar findings have been observed by Liao *et al.* [56] for 7.5 MRad GUR 1020 polymer articulating against polished CoCr roughened to R_a ~0.040 μm. It is not known whether an extended duration of testing would lead to further scratching of the Ti-6Al-4V surface and whether this may result in scratches with a higher magnitude lip height, which may accelerate UHMPWE wear [57].

The friction coefficient for UHMWPE on Ti-6Al-4V was found to be 0.07 in the current study, which aligns well with the friction coefficient ranges reported in the literature between 0.06 and 0.11 [49,58,59]. UHMWPE on CoCr had the lowest friction coefficient of 0.03, among all material pairs (see Fig. 16), which aligns with friction coefficient ranges of 0.03–0.05 reported in literature [59,60]. Lower friction coefficients can be associated with improved wear performance [59], however, wear

of Ti-6Al-4 V/UHMWPE and CoCrMo/UHMWPE couples is dependent on multiple factors [54] and is not governed by friction alone.

A study by Cremer *et al.* [52], with conventional UHMWPE plates and thermally oxidised LPFB Ti-6Al-4V pins at a $CS = 0.1$ and $P = 2.53$ MPa yielded a K_f of 9.1E-7 mm^3 /Nm. In this investigation, the thermal oxidation step used in the processing of the pins resulted in a higher surface roughness ~0.250 μm. The reported wear in the current study at these specific test conditions can be estimated as $K_f = 4.05E\text{-}6$ mm^3 /Nm using the $K_f(CS, P)$ in Table 3. The difference in wear factors could be due to the different configuration of the material pairs when compared to this study (i.e., polymer pin on a metal plate versus metal pin on a polymer plate). Thus, the material pair configuration seems to play an important role in the wear of UHMWPE on BD-treated samples. It is argued that the polishing effect of the thermally oxidised Ti-6Al-4V was greater for the metal pins on polymer plates as a result of the smaller metal articulating surface, which is constantly in contact with the plate surface, thus resulting in the lower reported wear factor by Cremer *et al.* [52]. In addition, changing the material pair configuration alters the effective contact area of the polymeric component, leading to differences in the CS experienced, consequently influencing the expected wear.

The importance of utilising the BD-treatment was highlighted by the scratching and consequent increase in surface roughness of the untreated Ti-6Al-4V plates, after wear testing (Fig. 9). The articulating surface of BD-treated plates showed improved abrasion resistance and did not show signs of significant scratching after wear testing. Interestingly, the BD-treated plates showed improved wear behaviour over testing, due to the polymer polishing of the plates. It is reasoned that by improving the post-BD heat treatment surface roughness and maintaining an adequate thermal oxide layer thickness with good adhesion, the wear performance of UHMWPE on BD-treated Ti-6Al-4V would be improved. The thermal oxide layer grown during the boost diffusion process also holds additional benefits – especially within an implant biotribology setting. Some of these added benefits include enhanced corrosion resistance [12,13], biocompatibility [11], manufacturing of patient-specific implants through AM to match the mechanical properties of the patient's bone, weight optimisation, tailored articulating surfaces, and added features to enhance both bone in- and ongrowth [1, 3].

5. Limitations and future work

Several limitations should be considered when interpreting the findings from this simple-geometry pin-on-plate study. The study simplified *in-vivo* joint motions to a pin articulating on a plate, producing a near-constant contact pressure across the contact area, whereas real joints show a distribution of contact stresses and combined sliding-rolling kinematics that can alter wear behaviour [61]. Periodic cleaning of test samples could also remove any protective organic film that might form during testing. Protective biofilm formation is common in retrieved infected implants [62], and the wear and frictional properties of UHMWPE are highly dependent on both fungal and microbial contamination of the lubricant during wear testing [63]. Furthermore, this study did not evaluate whether the observed smoothing of the BD plate surfaces led to a loss of material.

Future work should focus on optimising BD-treated Ti-6Al-4V surfaces by refining polishing methods, reducing oxide grain clustering, and examining how the substrate microstructure influences oxide adhesion and surface roughness. Further studies could include fretting and tribocorrosion tests, varied wear couple orientations (e.g. metal pin on polymer plate), broader stress ranges, and alternative counterface materials to evaluate BD-treated Ti-6Al-4V across a wider range of implant applications.

6. Conclusions

This study assessed the wear behaviour of UHMWPE articulating against BD-treated AM Ti-6Al-4V across a controlled design space of cross-shear and contact stress. The findings show that, although BD treatment produces a hardened, oxygen-enriched surface layer in Ti-6Al-4V, this did not directly translate into improved wear performance under the multidirectional loading conditions investigated, with counterface wear instead being exacerbated by the associated surface roughness. In the absence of post-treatment polishing, this roughened topography largely governed the tribological response. The BD-treated surfaces generated noticeably higher UHMWPE wear rates than the untreated AM plates, driven primarily by asperity-level abrasion and the associated reduction in effective lubrication. These results are consistent with the mechanistic interpretation developed in the Discussion, where elevated roughness was identified as the principal factor exacerbating counterface wear. Further to this, the following main findings were made:

- Cross-shear had a strong influence on the wear factor, reflecting the established sensitivity of UHMWPE to multidirectional motion, whereas contact stress was the more influential parameter for friction and wear. The observed trends align with the known influence of crosslinking and contact mechanics on polymer wear, and the fitted response-surface models captured these dependencies within the bounds of the experimental design.
- Although the BD process produces a hard, oxygen-enriched surface layer that showed improved abrasion resistance of the Titanium alloy, the present results demonstrate that in the absence of post-treatment surface finishing, the resulting surface topography dominates the tribological response and leads to elevated wear rates. Prior work has shown that repolishing BD-treated Ti-6Al-4V can reduce roughness to values comparable with wrought materials; achieving such a finish would likely reverse the wear behaviour reported here and may enable superior tribological performance.
- This study demonstrates that, for AM Ti-6Al-4V, the BD heat treatment in its current form does not directly improve wear performance due to surface topography effects. While the resulting thermal oxide layer is known to offer advantages such as improved corrosion resistance and biocompatibility, these attributes do not mitigate the adverse tribological response observed here and require further investigation.

Overall, this work provides the first evaluation of UHMWPE wear against BD-treated AM Ti-6Al-4V under clinically relevant loading paths, identifies the surface-topography-driven mechanism responsible for the elevated wear observed, and delineates the treatment refinements required for future biomedical applications.

CRediT authorship contribution statement

L. Cremer: Writing – original draft, Visualization, Software, Methodology, Investigation, Formal analysis, Data curation, Conceptualization. **R.M. Cowie:** Writing – review & editing, Supervision, Methodology, Resources, Investigation Funding acquisition, Conceptualization. **J. van der Merwe:** Writing – review & editing, Supervision, Conceptualization. **L.M. Jennings:** Writing – review & editing, Supervision, Resources , Funding acquisition, Conceptualization. **T.H. Becker:** Writing – review & editing, Supervision, Funding acquisition, Conceptualization.

Statement of originality

As corresponding author, I Labau Cremer, hereby confirm on behalf of all authors that:

1. The paper has not been published previously, that it is not under consideration for publication elsewhere, and that if accepted it will not be published elsewhere in the same form, in English or in any other language, without the written consent of the publisher.
2. The paper does not contain material which has been published previously, by the current authors or by others, of which the source is not explicitly cited in the paper.

Declaration of Competing Interest

The authors declare that they have no known competing financial interests or personal relationships that could have appeared to influence the work reported in this paper.

Acknowledgements

The authors would like to acknowledge Orthoplastics for sponsoring a cross-linked GUR1020 polymer billet. The authors would also like to acknowledge funding from the Faculty of Engineering and Physical Sciences, International Academic Mobility Pump-priming Fund, University of Leeds, United Kingdom. Furthermore, the authors are grateful to the South African Department of Science and Innovation through the Collaborative Program for Additive Manufacturing (CPAM) administered by the Council for Scientific and Industrial Research (CSIR) for the project funding.

Data availability

The data associated with this article is openly available at https://doi.org/10.25413/sun.28445333.v1.

References

[1] Bose S, Ke D, Sahasrabudhe H, Bandyopadhyay A. Additive manufacturing of biomaterials. Prog Mater Sci 2018;93:45–111. https://doi.org/10.1016/j.pmatsci.2017.08.003.
[2] Tilton M, Lewis GS, Manogharan GP. Additive manufacturing of orthopedic implants. Orthopedic Biomaterials: Progress in Biology, Manufacturing, and Industry Perspectives. Springer International Publishing; 2018. p. 21–55. https://doi.org/10.1007/978-3-319-89542-0_2.
[3] Aufa AN, Hassan MZ, Ismail Z. Recent advances in Ti-6Al-4V additively manufactured by selective laser melting for biomedical implants: Prospect development. J Alloy Compd 2022;896:163072. https://doi.org/10.1016/j.jallcom.2021.163072.
[4] Kovács Á.É., Csernátony Z., Csámer L., Méhes G., Szabó D., Veres M., et al. Comparative Analysis of Bone Ingrowth in 3D-Printed Titanium Lattice Structures with Different Patterns 2023. https://doi.org/10.3390/ma16103861.
[5] Leary M. Design of titanium implants for additive manufacturing. Titanium in Medical and Dental Applications. Elsevier; 2018. p. 203–24. https://doi.org/10.1016/B978-0-12-812456-7.00009-3.
[6] Dong H, Bell T. Enhanced wear resistance of titanium surfaces by a new thermal oxidation treatment. Wear 2000;238:131–7. https://doi.org/10.1016/S0043-1648(99)00359-2.
[7] Dong H, Li XY. Oxygen boost diffusion for the deep-case hardening of titanium alloys. Materials Science Engineering A 2000;280:303–10. https://doi.org/10.1016/S0921-5093(99)00697-8.
[8] Dong H, Bell T. Enhanced wear resistance of titanium surfaces by a new thermal oxidation treatment. Wear 2000;238:131–7. https://doi.org/10.1016/S0043-1648(99)00359-2.
[9] Chen H-T, Lin H-I, Chung C-J, Tang C-H, He J-L. Osseointegrating and phase-oriented micro-arc-oxidized titanium dioxide bone implants. J Appl Biomater Funct Mater 2021;19. https://doi.org/10.1177/22808000211006878.
[10] Li B, Zhang L, Li Y, Li H, Zhou L, Liang C, et al. Corrosion Resistance and Biological Properties of Anatase and Rutile Coatings on a Titanium Surface. Chem Lett 2019;48:1355–7. https://doi.org/10.1246/CL.190549.
[11] García-Alonso MC, Saldaña L, Vallés G, González-Carrasco JL, González-Cabrero J, Martínez ME, et al. In vitro corrosion behaviour and osteoblast response of thermally oxidised Ti6Al4V alloy. Biomaterials 2003;24:19–26. https://doi.org/10.1016/S0142-9612(02)00237-5.
[12] Siva D., Krishna R., Sun Y.. Thermally oxidised rutile-TiO 2 coating on stainless steel for tribological properties and corrosion resistance enhancement 2005. https://doi.org/10.1016/j.apsusc.2005.02.046.
[13] Pejakovi V., Totolin V., Ripoll R. Tribocorrosion behaviour of Ti6Al4V in artificial seawater at low contact pressures 2017. https://doi.org/10.1016/j.triboint.2017.10.025.
[14] Casadebaigt A, Hugues J, Monceau D. Influence of Microstructure and Surface Roughness on Oxidation Kinetics at 500–600 °C of Ti–6Al–4V Alloy Fabricated by Additive Manufacturing. Oxid Met 2018;90:633–48. https://doi.org/10.1007/S11085-018-9859-0.
[15] Dickes D, Öztürk B, Völkl R, Galetz MC, Glatzel U. Improving the Adhesion of a Hard Oxide Layer on Ti6Al4V by a Three-Step Thermal Oxidation Process. Adv Eng Mater 2022;24. https://doi.org/10.1002/adem.202100864.
[16] Zhang ZX, Dong H, Bell T, Xu B. The effect of treatment condition on boost diffusion of thermally oxidised titanium alloy. J Alloy Compd 2007;431:93–9. https://doi.org/10.1016/J.JALLCOM.2006.05.045.
[17] Jiang Y, Mao H, Xiaowei W, Lu Y, Gong J. Effect of oxygen boost diffusion treatment on the mechanical properties of Ti-6Al-4V alloy. Surf Interfaces 2021;25:101248. https://doi.org/10.1016/J.SURFIN.2021.101248.
[18] Dickes D, Öztürk B, Völkl R, Galetz MC, Glatzel U. Improving the adhesion of a hard oxide layer on Ti6Al4V by a three-step thermal oxidation process. Adv Eng Mater 2022;24. https://doi.org/10.1002/adem.202100864.
[19] Dong H, Li XY. Oxygen boost diffusion for the deep-case hardening of titanium alloys. Materials Science Engineering A 2000;280:303–10. https://doi.org/10.1016/S0921-5093(99)00697-8.
[20] Cremer L, van der Merwe J, Becker TH. Oxygen boost diffusion of additively manufactured Ti-6Al-4V for improved oxide layer adhesion. J Alloy Compd 2025;1031:180857. https://doi.org/10.1016/J.JALLCOM.2025.180857.
[21] ASTM F732-17. Standard Test Method for Wear Testing of Polymeric Materials Used in Total Joint Prostheses. 2017. https://doi.org/10.1520/F0732-17.
[22] Wang A. A unified theory of wear for ultra-high molecular weight polyethylene in multi-directional sliding. Wear 2001;248:38–47. https://doi.org/10.1016/S0043-1648(00)00522-6.
[23] Wang A, Sun DC, Yau SS, Edwards B, Sokol M, Essner A, et al. Orientation softening in the deformation and wear of ultra-high molecular weight polyethylene. Wear 1997;203-204:230–41. https://doi.org/10.1016/S0043-1648(96)07362-0.
[24] Turell M, Wang A, Bellare A. Quantification of the effect of cross-path motion on the wear rate of ultra-high molecular weight polyethylene. Wear 2003;255:1034–9. https://doi.org/10.1016/S0043-1648(03)00357-0.
[25] Kang L, Galvin AL, Fisher J, Jin Z. Enhanced computational prediction of polyethylene wear in hip joints by incorporating cross-shear and contact pressure in additional to load and sliding distance: effect of head diameter. J Biomech 2009;42:912–8.
[26] Pathania A, Subramaniyan AK, Nagesha BK. Influence of post-heat treatments on microstructural and mechanical properties of LPBF-processed Ti6Al4V alloy. Prog Addit Manuf 2022;7:1323–43. https://doi.org/10.1007/S40964-022-00306-6/FIGURES/27.
[27] Becker TH, Kumar P, Ramamurty U. Fracture and fatigue in additively manufactured metals. Acta Mater 2021;219:117240.
[28] Memon AR, Wang E, Hu J, Egger J, Chen X. A review on computer-aided design and manufacturing of patient-specific maxillofacial implants. Expert Rev Med Devices 2020;17:345. https://doi.org/10.1080/17434440.2020.1736040.
[29] Schroeder L, Dunaway A, Dunaway D. A Comparison of Clinical Outcomes and Implant Preference of Patients with Bilateral TKA: One Knee with a Patient-Specific and One Knee with an Off-the-Shelf Implant. JBJS Rev 2022;10. https://doi.org/10.2106/JBJS.RVW.20.00182.
[30] Jennison T, Dalgleish J, Sharpe I, Davies M, Goldberg A. Total talus replacements. Foot Ankle Orthop 2023;8. https://doi.org/10.1177/24730114221151068.
[31] Cowie RM, Briscoe A, Jennings LM. The influence of cross shear and contact pressure on the wear of UHMWPE-on-PEEK-OPTIMA™ for use in total knee replacement. J Mech Behav Biomed Mater 2023;148:106196. https://doi.org/10.1016/J.JMBBM.2023.106196.
[32] Cowie RM, Briscoe A, Fisher J, Jennings LM. Wear and friction of UHMWPE-on-PEEK OPTIMA$^{T.\ M}$ J Mech Behav Biomed Mater 2019;89:65–71. https://doi.org/10.1016/J.JMBBM.2018.09.021.
[33] Abdelgaied A, Brockett CL, Liu F, Jennings LM, Fisher J, Jin Z. Quantification of the effect of cross-shear and applied nominal contact pressure on the wear of moderately cross-linked polyethylene. Proc Inst Mech Eng H 2013;227:18–26.
[34] Kang L, Galvin AL, Brown TD, Jin Z, Fisher J. Quantification of the effect of cross-shear on the wear of conventional and highly cross-linked UHMWPE. J Biomech 2008;41:340–6.
[35] Galvin A, Kang L, Tipper J, Stone M, Ingham E, Jin Z, et al. Wear of crosslinked polyethylene under different tribological conditions. J Mater Sci Mater Med 2006;17:235–43. https://doi.org/10.1007/s10856-006-7309-z.
[36] Chen J, Akyuz U, Xu L, Pidaparti RMV. Stress analysis of the human temporomandibular joint. Med Eng Phys 1998;20:565–72.
[37] Shao B, Teng H, Dong S, Liu Z. Finite element contact stress analysis of the temporomandibular joints of patients with temporomandibular disorders under mastication. Comput Methods Prog Biomed 2022;213. https://doi.org/10.1016/j.cmpb.2021.106526.
[38] Zhu Y, Zheng F, Gong Y, Zhu J, Yin D, Liu Y. Effect of occlusal contact on TMJ loading during occlusion: An in silico study. Comput Biol Med 2024;178:108725. https://doi.org/10.1016/J.COMPBIOMED.2024.108725.
[39] Anderson DD, Goldsworthy JK, Li W, Rudert MJ, Tochigi Y, Brown TD. Physical validation of a patient-specific contact finite element model of the ankle. J Biomech 2007;40:1662–9.
[40] Brand RA. Joint contact stress: a reasonable surrogate for biological processes? Iowa Orthop J 2005;25:82–94.
[41] Yu J, Zhao D, Chen WM, Chu P, Wang S, Zhang C, et al. Finite element stress analysis of the bearing component and bone resected surfaces for total ankle replacement with different implant material combinations. BMC Musculoskelet Disord 2022;23:1–11. https://doi.org/10.1186/S12891-021-04982-3/FIGURES/8.

[42] Rickard Sjoegren. pyDOE2. PyPI 2018. ⟨https://pypi.org/project/pyDOE2/⟩ (accessed September 19, 2024).
[43] Abdelgaied A, Fisher J, Jennings LM. A comprehensive combined experimental and computational framework for pre-clinical wear simulation of total knee replacements. J Mech Behav Biomed Mater 2018;78:282–91. https://doi.org/10.1016/j.jmbbm.2017.11.022.
[44] Cremer L, van der Merwe J, Becker TH. A method for determining machine configurations for multidirectional pin-on-plate wear testing. Results Surf Interfaces 2025;19:100488. https://doi.org/10.1016/J.RSURFI.2025.100488.
[45] Cowie RM, Briscoe A, Jennings LM. The influence of lubricant temperature on the wear of total knee replacements. Biosurf Biotribol 2023;9:71–7. https://doi.org/10.1049/BSB2.12061.
[46] Mattei L, Di Puccio F, Ciulli E. A comparative study of wear laws for soft-on-hard hip implants using a mathematical wear model. Tribol Int 2013;63:66–77. https://doi.org/10.1016/j.triboint.2012.03.002.
[47] Forster H., Fisher J. The influence of continuous sliding and subsequent surface wear on the friction of articular cartilage. 1999.
[48] Abdelgaied A, Liu F, Brockett C, Jennings L, Fisher J, Jin Z. Computational wear prediction of artificial knee joints based on a new wear law and formulation. J Biomech 2011;44:1108–16. https://doi.org/10.1016/J.JBIOMECH.2011.01.027.
[49] Dong H, Shi W, Bell T. Potential of improving tribological performance of UHMWPE by engineering the Ti6Al4V counterfaces. Wear 1999;225-229:146–53. https://doi.org/10.1016/S0043-1648(98)00356-1.
[50] Wang A, Polineni VK, Stark C, Dumbleton JH. Effect of femoral head surface roughness on the wear of ultrahigh molecular weight polyethylene acetabular cups. J Arthroplast 1998;13:615–20. https://doi.org/10.1016/S0883-5403(98)80002-8.
[51] Brown TD, Stewart KJ, Nieman JC, Pedersen DR, Callaghan JJ. Local head roughening as a factor contributing to variability of total hip wear: a finite element analysis. J Biomech Eng 2002;124:691–8. https://doi.org/10.1115/1.1517275.
[52] Cremer L, Nortje BD, van der Merwe J, Becker TH. Wear of conventional UHMWPE articulating against additively manufactured Ti-6Al-4V and Co-Cr-Mo. Biotribology 2023:33–4. https://doi.org/10.1016/J.BIOTRI.2022.100231. 100231.
[53] Baykal D, Siskey RS, Haider H, Saikko V, Ahlroos T, Kurtz SM. Advances in tribological testing of artificial joint biomaterials using multidirectional pin-on-disk testers. J Mech Behav Biomed Mater 2014;31:117–34.
[54] Jin ZM, Stone M, Ingham E, Fisher J. Biotribology. Curr Orthop 2006;20:32–40. https://doi.org/10.1016/j.cuor.2005.09.005.
[55] Cybo J, Maszybrocka J, Barylski A, Kansy J. Resistance of UHMWPE to plastic deformation and wear and the possibility of its enhancement through modification by radiation. J Appl Polym Sci 2012;125:4188–96. https://doi.org/10.1002/APP.36573.
[56] Liao Y-S, Greer K, Alberts A. Effect of head material and roughness on the wear of 7.5 Mrad crosslinked-remelted UHMWPE acetabular inserts. 2008. Proceedings of the 54th Annual Meeting of the Orthopaedic Research Society.
[57] Cowie RM, Jennings LM. Third body damage and wear in arthroplasty bearing materials: A review of laboratory methods. Biomater Biosyst 2021;4:100028. https://doi.org/10.1016/J.BBIOSY.2021.100028.
[58] Ruggiero A, D'Amato R, Gómez E. Experimental analysis of tribological behavior of UHMWPE against AISI420C and against TiAl6V4 alloy under dry and lubricated conditions. Tribol Int 2015;92:154–61. https://doi.org/10.1016/J.TRIBOINT.2015.06.005.
[59] Guezmil M, Bensalah W, Mezlini S. Tribological behavior of UHMWPE against TiAl6V4 and CoCr28Mo alloys under dry and lubricated conditions. J Mech Behav Biomed Mater 2016;63:375–85. https://doi.org/10.1016/J.JMBBM.2016.07.002.
[60] Yao JQ, Laurent MP, Johnson TS, Blanchard CR, Crowninshield RD. The influences of lubricant and material on polymer/CoCr sliding friction. Wear 2003;255:780–4. https://doi.org/10.1016/S0043-1648(03)00180-7.
[61] Kang L, Galvin AL, Brown TD, Fisher J, Jin ZM. Wear simulation of ultra-high molecular weight polyethylene hip implants by incorporating the effects of cross-shear and contact pressure. Proc Inst Mech Eng H 2008;222:1049–64. https://doi.org/10.1243/09544119JEIM431.
[62] Donlan RM. New approaches for the characterization of prosthetic joint biofilms. Clin Orthop Relat Res 2005;(437):12–9. https://doi.org/10.1097/01.BLO.0000175120.66051.29.
[63] Wimmer MA, Sah R, Laurent MP, Virdi AS. The effect of bacterial contamination on friction and wear in metal/polyethylene bearings for total joint repair—a case report. Wear 2013;301:264–70. https://doi.org/10.1016/J.WEAR.2012.11.022.